Interference between excitation routes in resonant sum-frequency mixing

Richard R. Moseley, Sara Shepherd, David J. Fulton, Bruce D. Sinclair, and Malcolm H. Dunn
J. F. Allen Physics Research Laboratories, Department of Physics and Astronomy, University of St. Andrews, St. Andrews, Fife KY16 9SS, Scotland
(Received 21 April 1994)

We present theory and observation to show that in resonant sum-frequency mixing the two pathways to the excitation of the coherence driving the output may be controlled in relative strength, and combine in antiphase on resonance. These two pathways are, first, a two-step route resulting in the creation of a real intermediate population, and second, a direct two-photon excitation resonantly enhanced by, but not populating, the intermediate level. The former route is shown to be raised over the latter by use of a stronger lower laser field. Experimental observation uses the $3S$-$3P_{1/2}$-$3D$ level scheme in sodium vapor and single-frequency continuous-wave lasers for steady-state conditions and high resolution. A cancellation ratio of 94% is reported. Further, noninterfering incoherent fluorescence and an anti-Stokes Raman process are observed and contrasted.

PACS number(s): 42.65.Ky, 42.50.Gy, 42.65.Dr, 32.80.−t

I. INTRODUCTION

It has been appreciated for some time that for a three-cascade-level atom excited by two resonant fields there are two routes available to populate the upper level [1]. One is a "two-step" process involving the creation of an intermediate level population, and the other a direct "two-photon" transition resonantly enhanced by the intermediate level, but not populating it. The split is useful in dealing with collisional effects but with a low level of such perturbations any discrimination is somewhat academic as the two routes are inseparable [1,2]. In this paper we report that these routes may, however, interfere in sum-frequency mixing (SFM) and should always be separately considered in this context. The coherence that drives the SFM output is contributed to, on resonance, in antiphase by the two paths and, moreover, the relative strengths of the routes can be varied by the pump field powers as well as their detunings. During SFM the two routes are associated with different broadening and resonance conditions. In a vapor cell the two-step route is velocity selective while the two-photon route is Doppler broadened. While the upper-state population shows both features as well, they are not purely associated with one route path and the relative strengths of the sub-Doppler and Doppler components are determined only by the detunings and not the input laser powers.

An atomic vapor may be a useful medium for a second-order SFM process if the isotropy is broken by external means ([3,4], and references therein). One transition will be dipole-forbidden, but if quadrupole allowed may still lead to a strong nonlinearity [5]. We recently reported experiments on two routes for SFM in sodium vapor [6] where the intermediate level was detuned far in excess of the Doppler width. We have extended the study using the $3S$-$3P$-$3D$ level scheme but now for the situation of simultaneous single- and two-photon resonance retaining the use of continuous-wave (cw) lasers for high spectroscopic resolution. The two routes of excitation of the upper level are clearly separated by their different linewidths and by varying the relative laser powers it is possible to make either one dominate in the output, and in the intermediate case interference is clearly visible. The interference arises as the two routes lead to opposing phases in the excitation of the coherence driving the SFM process and we will show by density-matrix calculations for a three-level atom the origin of this effect. As opposed to other quantum interference processes observable in atomic coherences such as electromagetically induced transparency (EIT) [7–10] there is no power threshold for the observation of this interference. It is the *relative* route strengths that are important, which may be changed by independently altering the input laser strengths or the detuning from single-photon resonance. There is, however, a comparison to be made here between EIT or Fano interference and this work; all of these systems produce interference as the result of two paths leading to the same end.

Furthermore, we have observed strong anti-Stokes Raman output at the same wavelength as the SFM signal. A quadrupole Raman process has been observed before in potassium vapor [11,12] but with the exciting radiation on the quadrupole transition and using pulsed excitation. Our experiment differs substantially from this. First, it is continuous wave; second, the process is quadrupole anti-Stokes, and further the two-step and two-photon routes can been identified in the output. This process, like that of population of the upper level, does not display interference in the two routes and the splittings of the various velocity-selected features are the same as for the fluorescence or SFM. Figure 1 shows the three processes discussed in this work: population of the upper level (monitored by fluorescence); the creation of the SFM coherence between the $3S$ and $3D$ states; and anti-Stokes Raman conversion. The nature of the Raman process is an excitation to the $3P$ level by the first laser followed by some

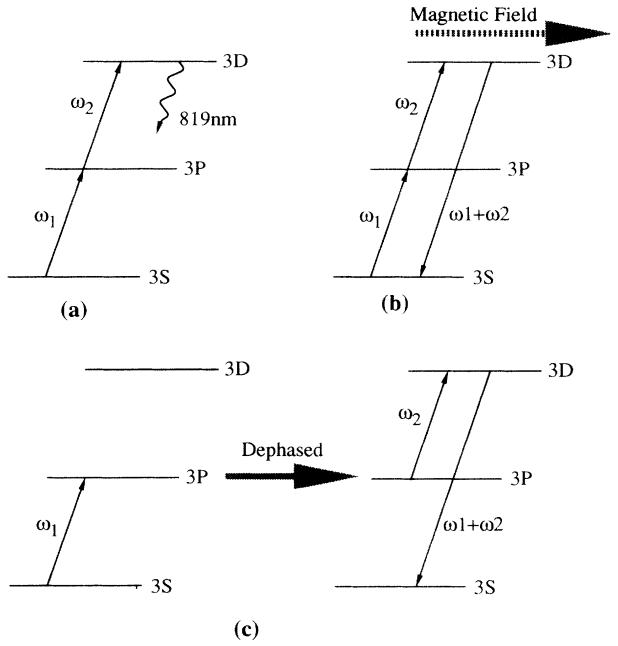

FIG. 1. A schematic of the three processes observed: (a) upper-level spontaneous decay, (b) resonant magnetic-field-induced sum-frequency mixing, and (c) anti-Stokes Raman conversion.

dephasing process, most probably collisional. Thereafter, the second laser initiates a Raman conversion to shorter wavelengths which is enhanced by the resonance with a dipole-allowed ($3P$-$3D$) and then quadrupole-allowed ($3D$-$3S$) transition.

The Raman and sum-frequency processes may be readily separated by use of the transverse magnetic field. If this is removed the second-order SFM signal is removed allowing clear observation of the third-order Raman signal. Once the magnetic field is applied both signals are present but SFM may dominate under appropriate vapor conditions, detailed later.

In Sec. II of this paper we detail solutions of the density-matrix approach for a three-level atom displaying the route interference mentioned above. Its origin is discussed and the effect of the laser strengths and single-photon detuning detailed with respect to the features in the observable output line shape. Thereafter we detail the experiment in Sec. III and then results for the nonparametric processes in Sec. IV showing the two excitation features. The contrasting SFM signals are discussed in Sec. V and the interference features observed compared to theory.

II. THEORY

In order to predict the SFM coherence between the ground state and the uppermost level we must calculate the slowly varying off-diagonal matrix element $\tilde{\rho}_{13}$ by solution of the coupled density matrix equations for a three-level atom. We consider a cascade atom (of the form of Fig. 2) and assume that fields ω_1 and ω_2 are injected from single-mode cw laser sources and are close in frequency to only one transition. We define

$$E(\omega_i,t)=\frac{1}{2}E_i\{\exp[i(\omega_i t+k_i z)]+\text{c.c.}\} \tag{1}$$

as the description of the electric fields, which will lead to half Rabi frequencies, on the appropriate transition of matrix element μ_{jk}, of

$$\Omega_i=\frac{\mu_{jk}E_i}{2\hbar}. \tag{2}$$

Proceeding from the Liouville equation [13,14] we obtain the evolution of the density-matrix components as follows:

$$\dot{\rho}_{11}=i\Omega_1(\tilde{\rho}_{21}-\tilde{\rho}_{12})+\Gamma_{21}\rho_{22}, \tag{3a}$$

$$\dot{\rho}_{22}=i\Omega_1(\tilde{\rho}_{12}-\tilde{\rho}_{21})+i\Omega_2(\tilde{\rho}_{32}-\tilde{\rho}_{23})-\Gamma_{21}\rho_{22}+\Gamma_{32}\rho_{33}, \tag{3b}$$

$$\dot{\rho}_{33}=i\Omega_2(\tilde{\rho}_{23}-\tilde{\rho}_{32})-\Gamma_{32}\rho_{33}, \tag{3c}$$

$$\dot{\tilde{\rho}}_{12}=-i(\Delta_1-i\gamma_{12})\tilde{\rho}_{12}+i\Omega_1(\rho_{22}-\rho_{11})-i\Omega_2\tilde{\rho}_{13}, \tag{3d}$$

$$\dot{\tilde{\rho}}_{23}=-i(\Delta_2-i\gamma_{23})\tilde{\rho}_{23}+i\Omega_2(\rho_{33}-\rho_{22})+i\Omega_1\tilde{\rho}_{13}, \tag{3e}$$

$$\dot{\tilde{\rho}}_{13}=-i(\Delta_1+\Delta_2-i\gamma_{13})\tilde{\rho}_{13}+i\Omega_1\tilde{\rho}_{23}-i\Omega_2\tilde{\rho}_{12}. \tag{3f}$$

Within these, the detunings are defined as $\Delta_i=\omega_i-k_iV_z-\omega_{i(i+1)}$ with the k_iV_z term taking account of the Doppler shift due to motion in the z direction. The population decay rates are Γ_{ij} while the coherence decay rates are denoted γ_{ij}. We have assumed, without loss of generality, that the Rabi frequencies Ω_i are real. Optical frequency oscillations of the off-diagonal elements have been removed by the substitutions:

$$\rho_{12}=\tilde{\rho}_{12}\exp[i(\omega_1 t+k_1 z)], \tag{4a}$$

$$\rho_{23}=\tilde{\rho}_{23}\exp[i(\omega_2 t+k_2 z)], \tag{4b}$$

$$\rho_{13}=\tilde{\rho}_{13}\exp[i\{(\omega_1+\omega_2)t+(k_1+k_2)z\}]. \tag{4c}$$

For sum-frequency mixing in this system the important matrix element is the coherence between the uppermost and the ground state, $\tilde{\rho}_{13}$, while previous treatments have tended to concentrate on the upper state population, ρ_{33}. Berman [1] gives six chains leading to ρ_{33}, of which two are identified as "two quanta" and do not involve the

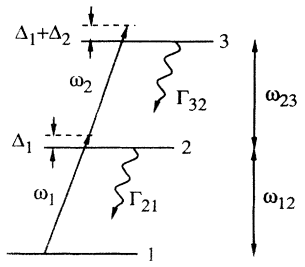

FIG. 2. A cascade three-level atom.

creation of a finite ρ_{22} and four are "two step" and do involve the creation of a finite ρ_{22}. They are symmetric in their use of the fields, all being of order $(\Omega_1\Omega_2)^2$. However, in the absence of strong collisional perturbation of level 2 the split in routes is noted to be artificial and the result reduces to the expression derived from use of probability amplitudes where the two routes cannot be distinguished [2]. Doppler integration of the resulting expression leads to a mixed feature with both Doppler and velocity selected components. The relative importance of the two features are, hence, set only by the Maxwellian velocity distribution which determines how many atoms may have the correct Doppler shift for double resonance.

However, for SFM and the generation of $\tilde{\rho}_{13}$ the split into the different routes is important as the two routes have different input field dependences. In a similar manner to Berman we may look at the perturbation chains which the two routes follow. The two chains for the generation of $\tilde{\rho}_{13}$ by direct two-photon excitation are

$$\rho_{11} \overset{\Omega_1}{\rightarrow} \tilde{\rho}_{12} \overset{\Omega_2}{\rightarrow} \tilde{\rho}_{13}, \tag{5a}$$

$$\rho_{11} \overset{\Omega_1}{\rightarrow} \tilde{\rho}_{21} \overset{\Omega_2}{\rightarrow} \tilde{\rho}_{31}, \tag{5b}$$

while by two-step excitation the four relevant chains are

$$\rho_{11} \overset{\Omega_1}{\rightarrow} \tilde{\rho}_{12} \overset{\Omega_1}{\rightarrow} \rho_{22} \overset{\Omega_2}{\rightarrow} \tilde{\rho}_{23} \overset{\Omega_1}{\rightarrow} \tilde{\rho}_{13}, \tag{6a}$$

$$\rho_{11} \overset{\Omega_1}{\rightarrow} \tilde{\rho}_{21} \overset{\Omega_1}{\rightarrow} \rho_{22} \overset{\Omega_2}{\rightarrow} \tilde{\rho}_{23} \overset{\Omega_1}{\rightarrow} \tilde{\rho}_{13}, \tag{6b}$$

$$\rho_{11} \overset{\Omega_1}{\rightarrow} \tilde{\rho}_{12} \overset{\Omega_1}{\rightarrow} \rho_{22} \overset{\Omega_2}{\rightarrow} \tilde{\rho}_{32} \overset{\Omega_1}{\rightarrow} \tilde{\rho}_{31}, \tag{6c}$$

$$\rho_{11} \overset{\Omega_1}{\rightarrow} \tilde{\rho}_{21} \overset{\Omega_1}{\rightarrow} \rho_{22} \overset{\Omega_2}{\rightarrow} \tilde{\rho}_{32} \overset{\Omega_1}{\rightarrow} \tilde{\rho}_{31}. \tag{6d}$$

By this analysis we may now discern why $\tilde{\rho}_{13}$ may react differently to the two routes compared to the population, ρ_{33}. Whereas, for the population the routes were equivalent in their use of the fields, now the two-step route is of order $\Omega_1^2(\Omega_1\Omega_2)$ and the two photon, $(\Omega_1\Omega_2)$. Therefore, the two-step route is more sensitive to an increase in Ω_1 than the other route and will lead to the velocity-selecting route dominating for $\Omega_1 \gg \Omega_2$. However if the reverse is true the two-photon route may dominate *even on single-photon resonance*, a situation never true for the population [2].

Having illustrated the separation of these routes the possibility of interference may be elucidated by reference to Eq. (3f). Under steady-state conditions this may be written as

$$\tilde{\rho}_{13} = \frac{\Omega_1\tilde{\rho}_{23} - \Omega_2\tilde{\rho}_{12}}{(\Delta_{13} - i\gamma_{13})}. \tag{7}$$

The first term in the numerator is the last link in the chain of the two-step route while the latter is of the two-photon route. If we substitute for the coherences to first order this becomes

$$\tilde{\rho}_{13} = \frac{\Omega_1\Omega_2(\rho_{33} - \rho_{22})}{(\Delta_1 + \Delta_2 - i\gamma_{13})(\Delta_2 - i\gamma_{23})} - \frac{\Omega_1\Omega_2(\rho_{22} - \rho_{11})}{(\Delta_1 + \Delta_2 - i\gamma_{13})(\Delta_1 - i\gamma_{12})} \tag{8}$$

neglecting the higher order terms for $\tilde{\rho}_{13}$. If the excitation is of moderate strength in a Doppler broadened medium the populations will obey the relations: $\rho_{11} \approx 1$, $\rho_{22} \approx 0$, and $\rho_{33} \approx 0$. We may then deduce, using Im{ } to denote the imaginary part,

$$\tilde{\rho}_{13} = -\frac{2\Omega_1^3\Omega_2}{\Gamma_{21}(\Delta_1 + \Delta_2 - i\gamma_{13})(\Delta_2 - i\gamma_{23})}\mathrm{Im} \times \left\{\frac{1}{(\Delta_1 - i\gamma_{12})}\right\} + \frac{\Omega_1\Omega_2}{(\Delta_1 + \Delta_2 - i\gamma_{13})(\Delta_1 - i\gamma_{12})}. \tag{9}$$

To illustrate the properties and effects of the two terms of Eq. (9) it was split and these terms integrated individually by numerical means for Doppler broadening with $\Delta_1 = 0$. The resulting real and imaginary parts are displayed in Figs. 3(a) and 3(b), respectively. The different broadening natures of the two routes are clearly visible and the combination of field strengths was chosen to illustrate near cancellation.

In order to gain insight into the general shape of the output line shape with arbitrary detunings it is useful to

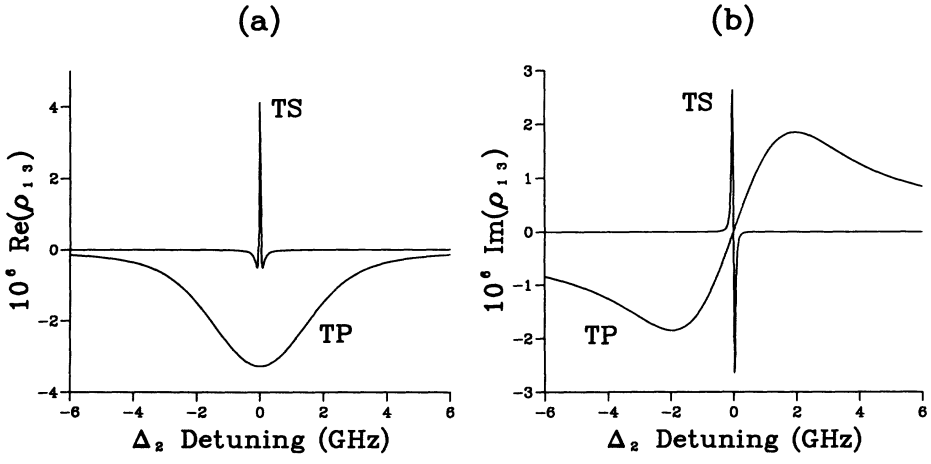

FIG. 3. Separate solutions of the two terms of Eq. (9), corresponding to the two-step (TS) and two-photon (TP) routes, split into (a) real and (b) imaginary parts and integrated over the velocity distribution at 500 K. (Other parameters are $\Omega_1 = \Omega_2 = 0.001$ GHz; $\Gamma_{32} = \Gamma_{21} = 0.05$ GHz; $\gamma_{12} = \gamma_{23} = 0.025$ GHz; $\gamma_{13} = 0.01$ GHz; $\Delta_1 = 0$.)

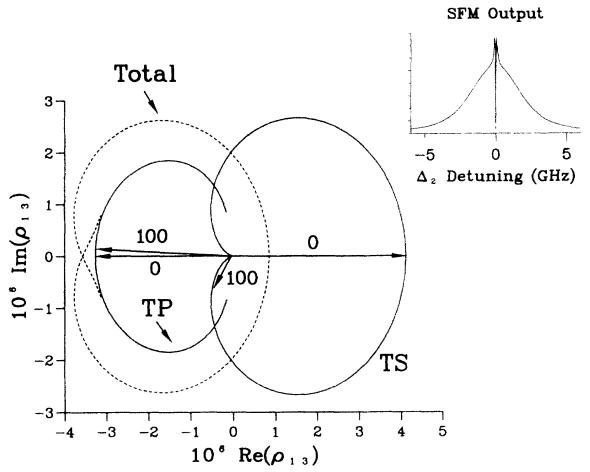

FIG. 4. The locus of points swept out by the phasors for each of the terms in Eq. (9), and the resulting total phasor for the parameters of Fig. 3. Phasor arrows are displayed for $\Delta_2 = 0$ and $\Delta_2 = 100$ MHz. The observable, the SFM line shape, is taken as proportional to $|\tilde{\rho}_{13}|^2$, and shown as an inset.

consider the phasors generated by each of the two terms in Eq. (9). The set of points mapped out by the phasors corresponding to the above example is shown in Fig. 4, with the observable, $|\tilde{\rho}_{13}|^2$, as an inset. The two phasors are in exactly opposite directions only on double resonance (as shown by the arrows labeled "0"). A vector addition must be carried out at all other points for the resultant output phasor lobe, shown by the dashed line. It is immediately obvious that the two routes' phasor lobes are mainly in the opposite sense but, as indicated by the phasors for an upper field detuning of 100 MHz (shown by the arrows labeled "100"), the phasors rotate in opposite directions. Furthermore, due to the substantially narrower linewidth the two-step (TS) phasor rotates much faster and only has significant effect on the output for the short range where the total phasor lobe deviates from the two-photon (TP) one. In this example the relative routes' strengths are such that the total output phasor rotates swiftly around to be parallel to the TS phasor at $\Delta_2 = 0$ and, thus, a sharp dip is seen in the output line shape. If the TS route were stronger the total output phasor lobe would extend closer to the TS phasor lobe at upper level resonance and a sharp peak would be seen with flanking minima as the phasor rotates from the TP orientation around, close to the origin, and over to the TS phase.

When Δ_1 is a finite value this method of visualization is at its most useful. An example with $\Delta_1 = 2$ GHz is used here, and shown in Figs. 5 and 6. Figure 5 displays the relative term strengths in an analogous way to Fig. 3, whereas Fig. 6 shows the resultant phasor lobes. The smaller magnitude of the TS route is clear and the corresponding phasor lobe is small, but of the same shape and orientation as the TS one in Fig. 4. However, the TP phasor lobe has been substantially rotated by the lower field offset and the two phasors are no longer directly opposing at $\Delta_2 = 0$. At the appropriate range of Δ_2 where the two paths are both of significant magnitude the TP phasor direction is such that the TS route has a mainly additive effect on the total output phasor lobe, apart from a small double back. Therefore, the SFM output line shape displays a small, almost dispersive feature where the routes combine. At intermediate detunings higher than this the TP route can have fallen almost to zero before the TS route becomes of significant strength and so the combination is trivial and almost scalar in manner.

Full numerical solutions allow a closer approximation to the experimental situation with the assumptions used to attain Eq. (9) relaxed. The field strengths are raised to above the saturation level as they are in the experiment but the main features of the simplified case remain. The solutions are gained by setting the time derivatives to zero in Eqs. (3) and solving the system, with the complex conjugates of the off-diagonal elements, simultaneously. Numerical integration over the Maxwellian velocity distribution is carried out for each point. Figure 7 displays the predicted line shape of $|\tilde{\rho}_{13}|^2$ (which the SFM power is proportional to) for various values of Ω_2 against the detuning of the upper laser field, Δ_2. For these traces Δ_1 was set to zero so the peak of both routes occurs at $\Delta_2 = 0$. At low values of the upper

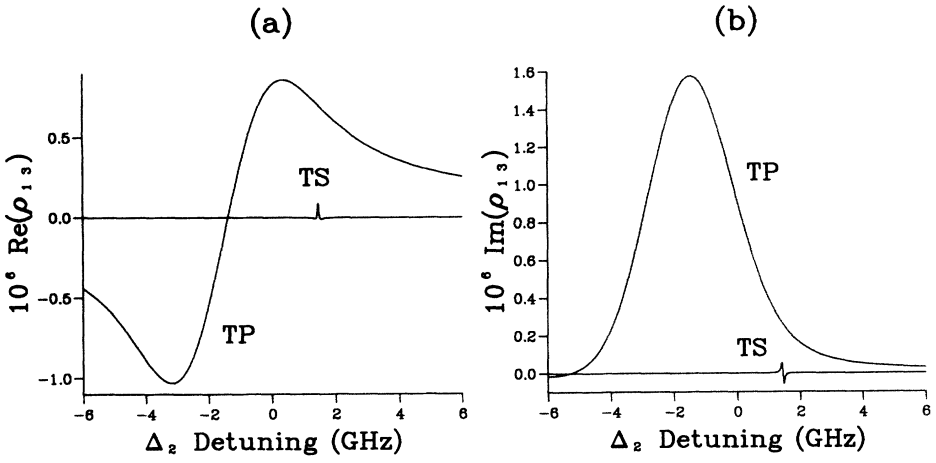

FIG. 5. Solutions of Eq. (9), as for Fig. 3, except with $\Delta_1 = 2$ GHz.

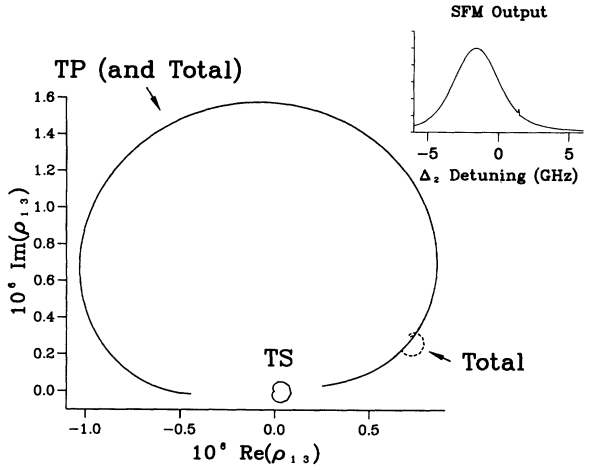

FIG. 6. Locus of points swept out by the phasors for each of the two terms of Eq. (9), as for Fig. 4, except for the parameters of Fig. 5.

field strength the velocity-selected route dominates and a narrow power broadened resonance is observed. As the upper field strength is increased the wings of the two-photon route build up to either side and sharp dips flank the two-step feature. These dips are due to the coherence swiftly changing phase from one route to the other and passing near the origin as it does. Eventually the strengths are such that the two routes exactly oppose on resonance and a complete cancellation is seen [see curve (d) in Fig. 7]. Thereafter, as the two-photon route continues to rise in magnitude the velocity-selected feature becomes a minimum in the profile. Similar distinctive features are obtained in reverse if Ω_2 is held constant and Ω_1 allowed to increase. However, the velocity-selected feature is seen to power broaden considerably within the Doppler profile as this field strength rises.

Behavior with different detuning offsets of Δ_1 is complex. The resonance positions of the two routes move across each other as the resonance condition for the two-photon route is $\Delta_2 = -\Delta_1$ while for the two-step route it is $\Delta_2 = \frac{k_2}{k_1}\Delta_1$. As the detunings change so do the relative route strengths and the profiles calculated are shown in Fig. 8. It is worth noting that at sufficient detuning of the lower laser ($\Delta_1 >$ Doppler width) no interference features can be observed and the profiles become similar to those predicted for the fluorescence.

III. EXPERIMENT

In order to observe this effect we have extended the experiment described in Ref. [6]. We have used two cw lasers, an argon-ion pumped dye laser (Spectra Physics

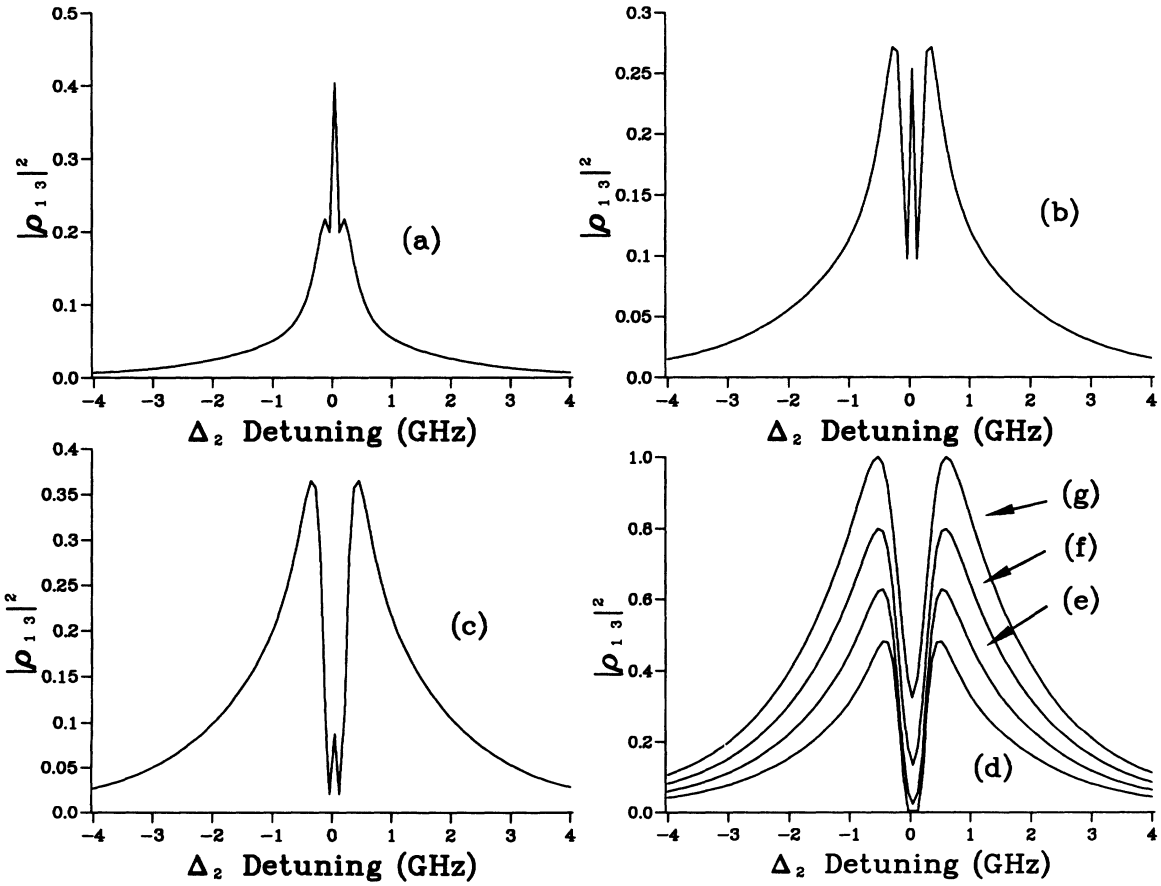

FIG. 7. Full numerical solutions for $|\tilde{\rho}_{13}|^2$ plotted against Δ_2 for $\Omega_1 = 0.02$ GHz and $\Omega_2 = 0.04, 0.06, 0.08, 0.10, 0.12, 0.14, 0.16$ GHz [traces (a) to (g), respectively].

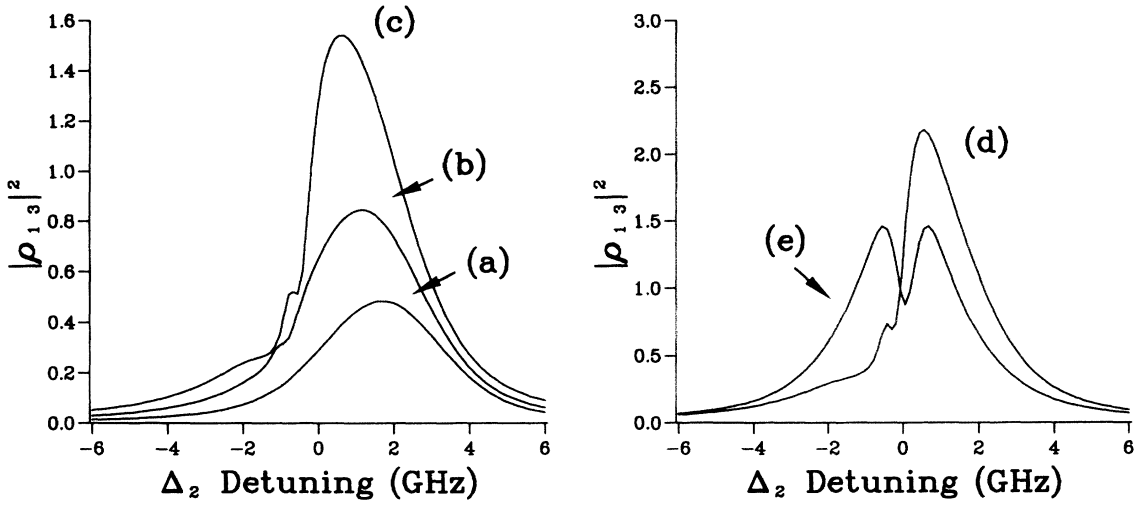

FIG. 8. Full numerical solutions for $|\tilde{\rho}_{13}|^2$ plotted against Δ_2 for $\Omega_1 = 0.02$ GHz, $\Omega_2 = 0.2$ GHz, and $\Delta_1 = -2, -1.5, -1, -0.5, 0$ GHz [traces (a) to (e), respectively].

380D) and a modified ring Ti:sapphire laser (Schwartz Electro-Optic Titan CW). The Ti:sapphire laser has been modified by the inclusion of an intracavity air-spaced étalon, a galvo-mounted solid étalon, and galvo-mounted brewster rhombs to allow for mode-hop free tuning via a dither and feedback technique. The lasers both produced single-frequency radiation, the former tunable around 589 nm ($3S$-$3P$) and the latter around 819 nm ($3P$-$3D$). During the experiment the dye laser was held steady in frequency while the Ti:sapphire scanned. This eased the experimental interpretation as the phase mismatch and the linear absorption of the dye laser field remained constant.

The outputs were combined and passed collinearly though an oven containing sodium and a small amount of argon buffer gas ($\approx$ 1 mbar). A transverse magnetic field could be applied across the vapor region by a Newport type-A electromagnet capable of providing a magnetic field up to 0.4 T in strength. The output radiation at 342 nm was detected by a photomultiplier tube (Hamamatsu 931B) after the fundamental radiation was filtered off by 2 UG11 filters. (A monochromator could be inserted after the oven, when required, to verify the output wavelength and all UV signals were ascertained to be close to the frequency of the $3D$-$3S$ transition.) Sideways 819-nm fluorescence, produced in a spectroscopic cell either separately or simultaneously to the experiments in the oven, served as a means for monitoring the line shape of excitation to the 3D level. The 589-nm beam was chopped and phase-sensitive detection used to raise the signal-to-noise level. The laser beams were unfocused and the vapor region is approximately 10 cm in length. Vapor temperatures of typically 180° C to 230 ° C were used (corresponding to sodium particle densities of around 10^{18} m^{-3} [15]).

IV. NONPARAMETRIC PROCESSES

While the level structure used in this work was not that of an ideal three-level atom, the interference effects were still obvious. Both the ground ($3S$) and intermediate ($3P$) states have appreciable hyperfine structure [16] with splittings of 1.77 GHz and 188 MHz, respectively. Selection rules do not permit excitation to the $3D_{5/2}$ level and any hyperfine structure is within the homogeneous linewidth for the $3D_{3/2}$ level [17]. The level scheme of interest is summarized in Fig. 9.

In order to probe spectroscopically the excitation of the sodium atoms to the 3D level two signals were used. The first was sideways fluorescence at 819 nm from the decay of the $3D$ state to the $3P$ state. With the dye laser tuned near resonance on the $3S$-$3P$ transition the line shape observed is shown in Fig. 10. Due to the velocity selection [2] the peak structures are observed separated not by their hyperfine splittings but incorporate a factor depending on the observing wave vectors. Table I summarizes the splittings expected and the velocity-selection factors. Observed splittings were consistent with these predictions.

The lines are strongly power broadened due to the laser powers being in excess of the saturation intensities for the transitions which mirror the conditions of the SFM experiment. Note how the two-step velocity-selected feature dominates here and increasing the Ti:sapphire laser power merely caused further power broadening. This is as predicted for the population in the upper level: Doppler broadening will not dominate with near resonant tuning for the lower laser, and high resolution spectroscopic information is received.

The second nonparametric signal observed was a UV signal at the $3D$-$3S$ wavelength, but with no magnetic

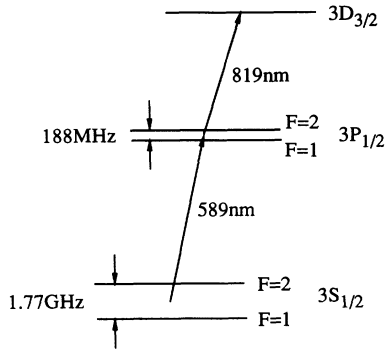

FIG. 9. Expanded detail of the hyperfine splitting in the $3S$-$3P_{1/2}$-$3D$ level scheme in sodium.

field applied across the vapor region. This was thought to be due to a $\chi^{(3)}$ quadrupole enhanced anti-Stokes Raman process. Fluorescence on this forbidden transition must be at a low level and the intensity in the forward direction was observed to be in excess of that to one side. The signal was also quite directional and observable up to 1 m away from the oven end. For input polarizations which were linear and parallel and in the absence of the magnetic field, selection rules do not allow excitation of the quadrupole moments able to radiate in the forward direction [18,19]. Therefore, we interpret the process as first an excitation via the dye laser to the $3P$ level followed by a dephasing process where the atomic orientation is lost. Then an excitation by the Ti:sapphire laser may occur where the appropriate quadrupole moment is coherently set up and forward 342-nm anti-Stokes radiation can occur. While second harmonic generation has been observed in a vapor without the application of a symmetry breaking field [20–22] we believe this signal is not due to sum-frequency mixing. This is because the mechanism required is thought to need high intensity pulses and a sensitive continuous-wave experiment [23] detected no parametric mixing processes. Furthermore, no phase matching oscillations were observed in the signal as the oven temperature was raised. Raman processes on a quadrupole resonance have been observed, however, in potassium vapor [11,12]. The efficiencies were quite high due to the low absorption associated with the quadrupole transition.

TABLE I. Corrections to observed structure due to velocity selection.

Level structure	$3S$	$3P$
Hyperfine splitting	1.77 GHz	188 MHz
Observation factor	$\frac{k_2}{k_1}$	$\left(1+\frac{k_2}{k_1}\right)$
Predicted observation	1.27 GHz	323 MHz

The line shape observed is the same as that for the fluorescence from the upper state, see Fig. 11. This suggests that the dephasing process does not perturb the velocity of the atom because if it did the velocity-selection process would be hindered. Behavior of the line shape with the upper laser power is shown in Fig. 12. As can be seen, the features merely power broaden at higher powers and the Doppler broadened background is not visible. As the dye laser is detuned progressively from resonance the expected behavior for the excitation to the $3D$ level is observed, Fig. 13. Only once the dye laser is detuned over 4 GHz does the peak of the two-photon route show through clearly. This behavior is typical of that expected for the excitation of population to the uppermost level and is altered only by the changing linear absorption on the dye laser as it is tuned across the single-photon resonance line.

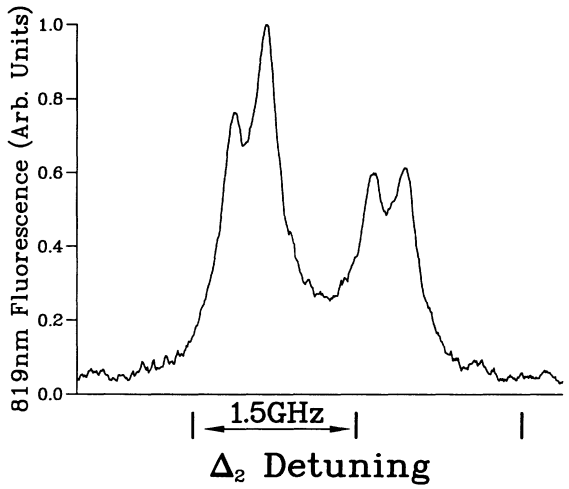

FIG. 10. Sideways 819-nm fluorescence observed from spontaneous decay of the $3D$ level as the Ti:sapphire laser was scanned across two-photon resonance. Laser powers were 90 mW (dye) and 100 mW (Ti:sapphire). A 1.5-GHz confocal marker was used to provide the frequency markers on the abscissa axis in this, and the other experimental figures.

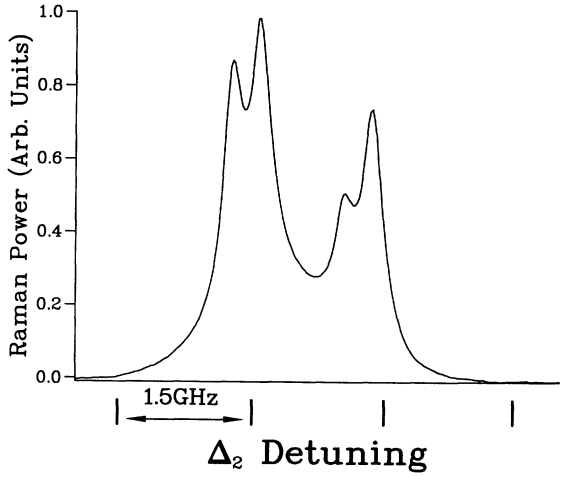

FIG. 11. The line shape of the anti-Stokes Raman process observed near 342 nm at the end of the sodium oven (vapor temperature $\approx$ 180 °C, and laser powers were both $\approx$ 20 mW).

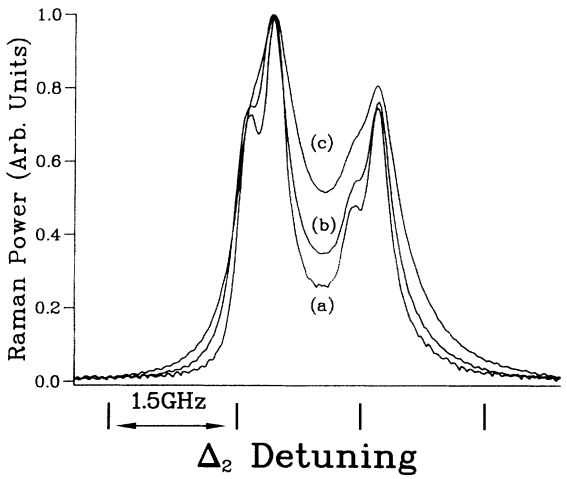

FIG. 12. Raman signal line shapes for Ti:sapphire laser powers of (a) 12.5 mW, (b) 50 mW, and (c) 200 mW normalized to the same peak height to show the power broadening (dye laser power 29 mW).

V. SUM-FREQUENCY MIXING

The line shapes observed for sum-frequency mixing are in sharp contrast to those displayed above due to the interference between the two paths. The SFM process was separated from the Raman process by the application of a small transverse magnetic field of typically 0.01 T. At vapor temperatures around 230 °C the SFM signal was an order of magnitude in excess of the zero field signal under these conditions.[1] Clear phase matching oscillations could be seen by detuning the dye laser by 8–10 GHz and raising the oven temperature. Under the conditions used in the experiment tuning of the Ti:sapphire laser did not produce any evidence of phase mismatching effects, as would be expected in the absence of a large intermediate population. Recent work on the phase matching properties of near-resonant SFM in sodium vapor [6] on an alternative route show how line shapes may be altered by phase mismatch but clean line profiles of both the two-step and two-photon routes were observed at the appropriate laser strengths for their dominance.

While the hyperfine structure of the sodium atom leads to two main clusters of Zeeman split routes, separated by the ground state sublevel spacing, it is possible to tune the dye laser to enhance one of these in the output and hence somewhat simplify the line shape. Figure 14 shows four such successive SFM line shapes against the upper laser scan for different laser powers. Quadrupling this laser power has the effect of doubling the Rabi frequency Ω_2 and thus enhancing the two-photon route. The first two traces show a narrow resonance from the two-step route on a low background with the stronger laser powers raising the two-photon route to prominence in later traces. The minima on either side of the main two-step

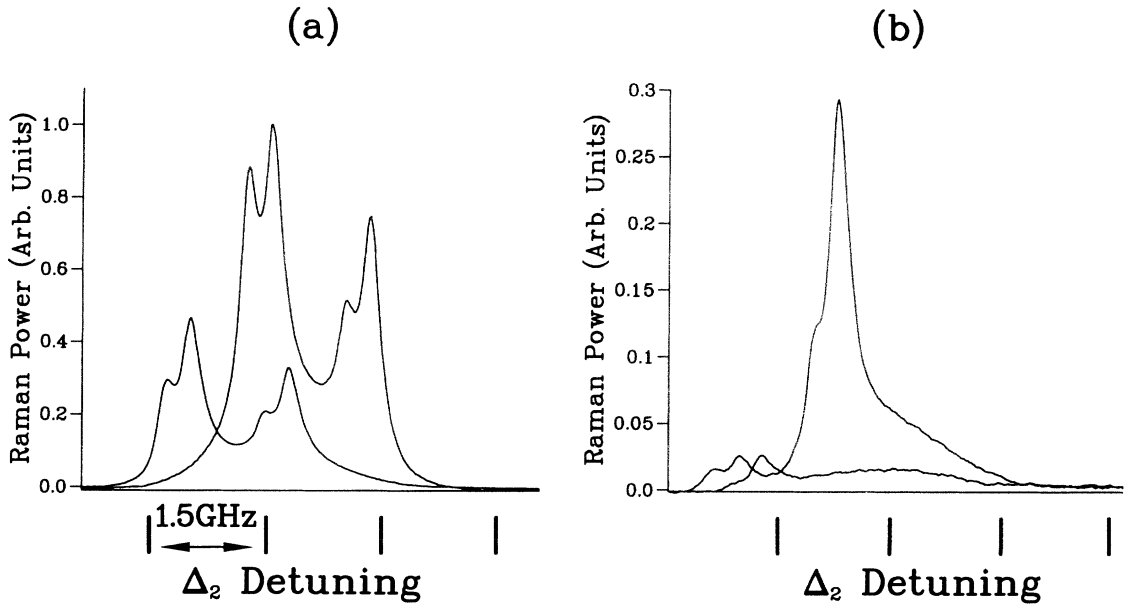

FIG. 13. Four Raman signal line shapes as the dye laser is detuned by successive 1.5-GHz intervals, starting with the larger trace in (a) and ending with the smaller trace in (b).

[1]It should be noted that using the $3S$-$3P_{3/2}$-$3D$ route this was not the case as the smaller hyperfine splittings in the $3P_{3/2}$ and greater number of routes reinforced the Raman signal.

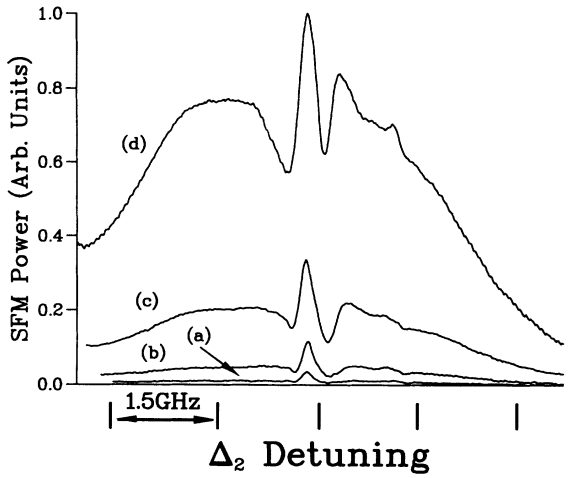

FIG. 14. Line shapes of the sum-frequency output observed as the Ti:sapphire laser is tuned for Ti:sapphire powers of (a) 3 mW, (b) 12.5 mW, (c) 50 mW, and (d) 200 mW (dye power 8 mW, vapor temperature $\approx$ 230 °C, transverse magnetic field of 0.013 T).

route cluster are direct evidence of the changing phase of the SFM driving coherence, as predicted in the theoretical results, e.g., Fig. 7. Indeed, this figure summarizes the main result of this paper: that the two routes may have opposite phase and that by changing the relative input powers the comparative route strengths may be altered.

At this laser tuning there was not sufficient available Ti:sapphire power to bring the two-photon route into dominance and see cancellation of the two routes. In order to do this the dye laser was detuned slightly. This has the effect of lowering the two-step route as the number of atoms in the correct velocity group for velocity selection is lowered due to the Maxwell-Boltzmann velocity distribution. By carefully adjusting the detuning and input powers, near cancellation could be achieved (Fig. 15). In this trace the two-step route can be seen

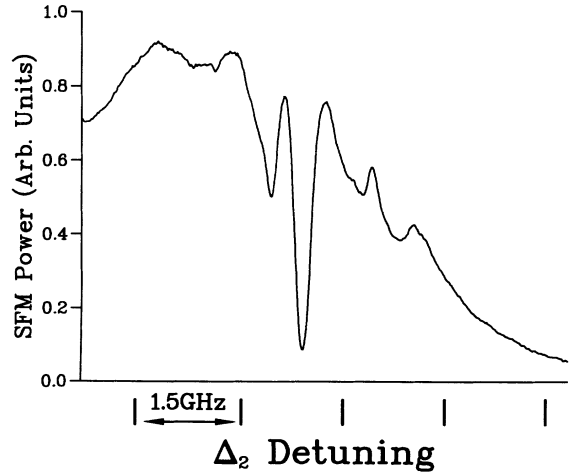

FIG. 15. Strong cancellation observed in the SFM line shape (dye 80 mW, Ti:sapphire 160 mW).

sunk into the two-photon profile with a strong cancellation to one side due to detuning effects. This feature is confirmed to be due to the opposing route phases by a halving of Ω_2 in Fig. 16. In this figure the two-photon route has now been lowered such that where the cancellation occurred before, a small peak is evident at the base of the minima. This is now the two-step route marginally outweighing the two-photon route and the feature is as predicted from theory (see Fig. 7). Theory would then predict this peak to grow in importance with decreasing upper laser power and it was indeed observed to do so. The maximum cancellation observed, measured as the distance between the peak of the two-photon route and the interference minimum was 94%. This is limited by the background Raman process, dominated but not removed, and the effects of linear absorption on Ω_1.

The behavior of the output with detuning of the lower laser, Δ_1, was complex. Not only do the relative route strengths vary rapidly but propagational effects such as linear absorption and phase mismatch do also. It was found that strong interference features were observed only within about a 1 GHz range of line center. Four successive traces as the dye laser was moved towards resonance are shown in Fig. 17. The line shapes at large detunings are similar to those for fluorescence or the Raman signal, where the two line shapes are superimposed on each other. This is again as predicted from theory. However, as close resonance approaches, the line shapes become rapidly more complicated as the route strengths and phases become important and interference effects distort the line shape.

VI. DISCUSSION AND CONCLUSIONS

While the experiments in sodium vapor serve to give functional fit to the theoretical predictions, if the hyperfine structure is appreciated, it would be desirable to gain a quantitative fit to theory by use of a three-level system

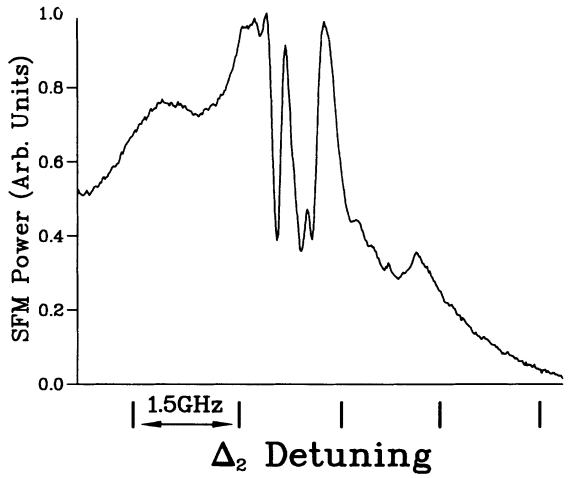

FIG. 16. As in Fig. 15 but with the Ti:sapphire power reduced to 40 mW to show the conditions where the two-step route now just outweighs the two-photon route at the cancellation point seen in the preceding figure.

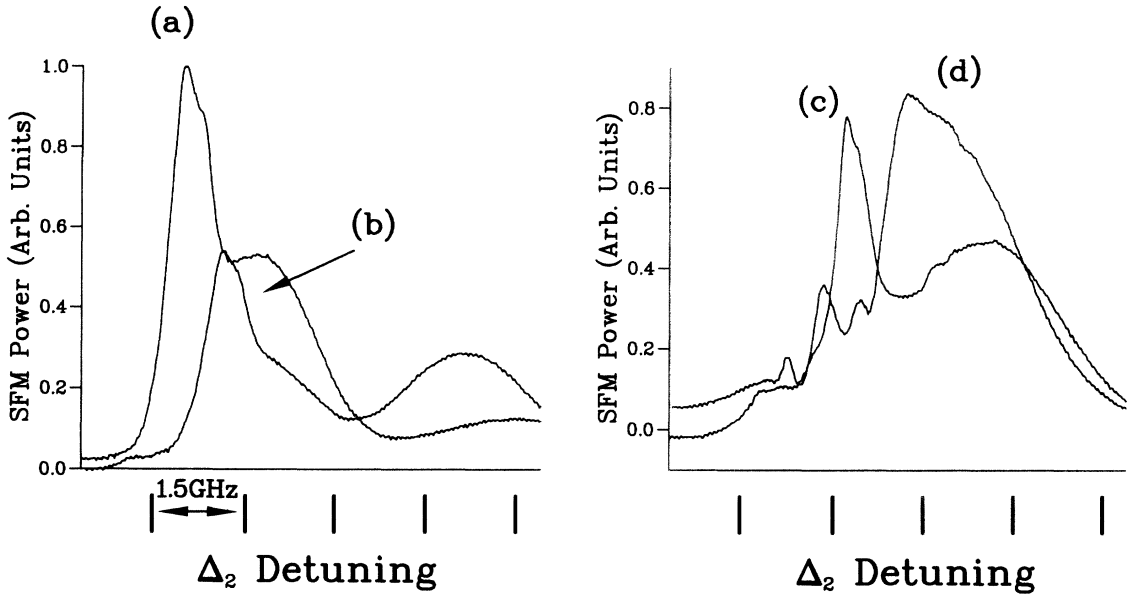

FIG. 17. Line shapes for the SFM output for successive 0.75 GHz moves of the dye laser detuning [(a) – (d)] (dye 8 mW, Ti:sapphire 50 mW).

without such additional structure. Alternatively, the role of the structure could be included in the modeling and a closer fit to the observed line shapes be demonstrated.

We believe that the interference process described and demonstrated in this work is fundamental to any *resonant* SFM process and is not restricted to the vapor phase. The behavior of atoms in a crystalline solid, for example, should be similar with the two-step route becoming site selective instead of velocity selective within the inhomogeneous lattice broadening. Furthermore, the interference process does not depend on some threshold value of an input power, which is the case in electromagnetically induced transparency (EIT). For EIT to be observed in a solid medium the Rabi splitting must be made in excess of the inhomogeneous broadening, implying very high, possibly damaging, intensities [9]. With route interference, low power lasers may be used, and indeed are favorable, due to the high resolution required.

The cancellation point, where the two routes are of equal strength, marks a delineation between two areas of resonant SFM behavior. When $\Omega_2 \ll \Omega_1$ the two-step route dominates and the SFM line shape is a useful sub-Doppler spectroscopic probe. The other region, where $\Omega_1 \ll \Omega_2$ is the domain where the efficiency of the nonlinear process may be greatly enhanced by EIT [10], provided that Ω_2 is in excess of the Doppler width. Numerical modeling shows that even if this latter condition is true, but the two-step route is still dominant, no enhancement in efficiency is observed. Modeling has also showed that cancellation between the routes is possible for Rabi frequencies both several times in excess of the Doppler width.

In conclusion therefore, we have described how the two-step route, involving the creation of an intermediate population, and the direct two-photon route for the generation of the SFM driving coherence may be controlled in relative magnitude and have opposing phases. The two-step route is dominant for higher values of the lower field Rabi frequency and the two-photon under opposite conditions. Incoherent fluorescence and an anti-Stokes Raman process provide a useful set of line shapes to set the SFM results against, highlighting the phenomena. While the theory and experiment were of direct relevance to isolated atoms in a vapor we believe these effects to be fundamental to any simultaneously single- and two-photon resonant SFM process.

ACKNOWLEDGMENTS

The authors wish to thank the Science and Engineering Research Council (SERC) for research funding at this time. Further, D.J.F and R.R.M. wish to acknowledge personal support from SERC and the Carnegie Trust for the Universities of Scotland, respectively.

[1] P. R. Berman, Phys. Rep. **43**, 101 (1978).
[2] J. E. Bjorkholm and P. F. Liao, Phys. Rev. A **14**, 751 (1976).
[3] N. Bloembergen, *Nonlinear Optics* (Benjamin, New York, 1965).
[4] A. J. Poustie and M. H. Dunn, Phys. Rev. A **47**, 1365 (1993).
[5] D. S. Bethune, R. W. Smith, and Y. R. Shen, Phys. Rev. Lett. **37**, 431 (1976).
[6] S. Shepherd, R. R. Moseley, B. D. Sinclair, and M. H.

Dunn, Phys. Rev. A **49**, 3002 (1994).
[7] K.-J. Boller, A. Imamoğlu, and S. E. Harris, Phys. Rev. Lett. **66**, 2593 (1991).
[8] J. E. Field, K. H. Hahn, and S. E. Harris, Phys. Rev. Lett. **67**, 3062 (1991).
[9] S. E. Harris, J. E. Field, and A. Imamoğlu, Phys. Rev. Lett. **64**, 1107 (1990).
[10] R. R. Moseley, B. D. Sinclair, and M. H. Dunn, Opt. Commun. **101**, 139 (1993).
[11] D. Cotter and M. A. Yuratich, Opt. Commun. **29**, 307 (1979).
[12] S. G. Dinev, G. B. Hadjichristov, and I. L. Stefanov, Opt. Commun. **74**, 176 (1989).
[13] A. Yariv, *Optical Electronics*, 3rd ed. (Holt-Saunders, New York, 1985).
[14] R. G. Brewer and E. L. Hahn, Phys. Rev. A **11**, 1641 (1975).
[15] R. B. Miles and S. E. Harris, IEEE J. Quantum Electron. **QE-9**, 470 (1973).
[16] E. Arimondo, M. Inguscio, and P. Violino, Rev. Mod. Phys. **49**, 31 (1977).
[17] B. Burghardt, B. Hoffmann, and G. Meisel, Z. Phys. D **8**, 109 (1988).
[18] B. D. Sinclair and M. H. Dunn, Phys. Rev. A **34**, 3989 (1986).
[19] M. Matsuoka, H. Nakatsuka, H. Uchiki, and M. Mitsunaga, Phys. Rev. Lett. **38**, 894 (1977).
[20] T. Mossberg, A. Flusberg, and S. R. Hartmann, Opt. Commun. **25**, 121 (1978).
[21] D. S. Bethune, Phys. Rev. A **23**, 3139 (1981).
[22] D. S. Bethune, Phys. Rev. A **25**, 2845(E) (1982).
[23] V. Mizrahi and D. P. Shelton, Phys. Rev. A **33**, 1396 (1986).

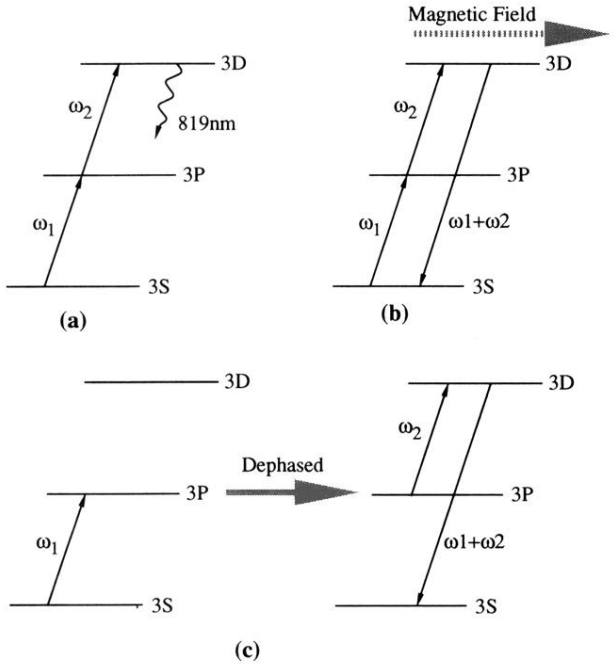

FIG. 1. A schematic of the three processes observed: (a) upper-level spontaneous decay, (b) resonant magnetic-field-induced sum-frequency mixing, and (c) anti-Stokes Raman conversion.